Highly Efficient Electrocatalytic Hydrogen Production by MoS_x Grown on Graphene-Protected 3D Ni Foams

*Yung-Huang Chang, Cheng-Te Lin, Tzu-Yin Chen, Chang-Lung Hsu, Yi-Hsien Lee, Wenjing Zhang, Kung-Hwa Wei, and Lain-Jong Li**

Hydrogen energy is clean and serves as one of the most promising candidates for replacing petroleum fuels in the future. Although the rare metals, such as platinum, have high efficiency in the hydrogen evolution reaction (HER), their scarcity and high cost inhibit large scale applications.[1–6] Recently, inorganic catalysts such as nanometer-scaled MoS_2 and WS_2 have drawn great attention due to their low cost, high chemical stability, and excellent photocatalytic[7–24] and electrocatalytic properties in HERs. They are potentially useful if they can be tailored for the development of hydrogen energy devices. In order to enhance the efficiency of inorganic catalysts, many research efforts have been made toward the modification of material properties,[25] the formation of composite catalysts,[26–31] and the fabrication of the electrodes with nano-architecture.[30–33] Recently, MoS_2/reduced graphene oxide catalyst composites have been successfully made for enhancing the electrocatalytic HER efficiency, where the reduced graphene oxide sheets serve the function of hosting MoS_2 as well as enhancing the conductance of the composites.[31,34] However, most of the reported electrode materials were still based on two-dimensional (2D) planar structures. To improve the electrocatalytic HER efficiency, it is crucial to effectively increase the surface area for catalyst loading. Hence, the research into three-dimensional (3D) electrode structures is emergent. A three-dimensional graphene foam synthesized on the Ni foam skeleton by chemical vapor deposition (CVD) has been reported.[36,37] The graphene foam without the support of an Ni skeleton is brittle and is not able to serve as a 3D electrode for hosting catalysts. The 3D Ni foam is a low cost and conductive metal with a high surface area, which is ideal for use as a template to host catalysts for increasing the number of reaction sites.[38–40] However, it suffers from instability in acidic solutions, and thus is not suitable for the electrocatalytic HER. Here, we report that the graphene sheets grown on Ni foams provide robust protection and efficiently increase their stability in acid. The highly conductive 3D graphene/Ni foam structure also effectively increases the catalyst loading, leading to the enhancement in electrocatalytic HER efficiency. Meanwhile, we formulated MoS_x ($x \geq 2$) catalytic materials on graphene-protected Ni foam to form a rigid 3D electrocatalytic architecture, where the MoS_x materials are grown by the thermolysis of ammonium thiomolybdates at different temperatures in a CVD chamber. The electrocatalytic HER of the MoS_x/graphene/3D Ni foam was performed in a 0.5 M H_2SO_4 solution. The HER current density for the MoS_x/graphene/3D Ni foam, either normalized by geometrical area or electrochemical surface area (ESA), is higher compared with the MoS_x on various planar carbon electrodes including carbon paper, carbon cloth, and graphene mats. X-ray photoelectron spectroscopy (XPS) analysis of the materials reveals that the higher HER efficiency is related to the presence of bridging S_2^{2-} or apical S^{2-} in amorphous states.

The three-dimensional Ni foam (110 ppi; thickness = 1.6 mm) was obtained from Nexcell battery Co. (Taiwan). The growth of a few layers of graphene on the Ni-foam by CVD has been reported elsewhere.[35] In brief, the Ni foams are reduced with H_2 flow (100 sccm) at 1050 °C for half an hour before the CVD growth (gas ratio CH_4:H_2 = 15:100; growth temperature 1050 °C for 1 h; pressure 500 mtorr). **Figure 1**a shows the scanning electron microscopy (SEM) images for the as-obtained Ni foam, where submillimeter pores can be clearly seen and the Ni grains of the skeletons are observable at a higher magnification. Figure 1b displays the SEM images after graphene layers are grown on the surfaces of Ni foam. The Ni surfaces are fully covered with graphene layers and the graphene wrinkles are clearly identified. The Raman spectrum in Figure S1, Supporting Information, proves that these graphene sheets are of a few layers. To grow MoS_x catalysts on the graphene surfaces, the graphene-protected Ni foam was immersed in an ammonium thiomolybdate solution (5 wt% of $(NH_4)_2MoS_4$ in DMF). The Ni foam was then backed on a hot plate at 100 °C for 10 min. The MoS_x layer was then formed after subsequent annealing at various temperatures (100, 120, 170, 200, 250, 300 °C) in a H_2/Ar environment (500 torr; H_2:Ar = 20:80) for 20 min. Figure 1c shows SEM images of the graphene-protected Ni foam grown with the MoS_x annealed at 120 °C. These images suggest that the MoS_x layer exhibits almost full coverage over the graphene surfaces, demonstrating that efficient loading of MoS_x on 3D Ni foam is achievable. The high resolution SEM image in Figure 1d reveals that the surface of the deposited MoS_x materials is very rough, and the MoS_x materials are composed of nanometer-scaled structures with large amounts of edges. The

Dr. Y.-H. Chang, Dr. C.-T. Lin, T.-Y. Chen, Dr. Y.-H. Lee, Dr. W. Zhang, Dr. L.-J. Li
Institute of Atomic and Molecular Sciences
Academia Sinica, Taipei 10617, Taiwan, ROC
E-mail: lanceli@gate.sinica.edu.tw
C.-L. Hsu, Dr. K.-H. Wei
Department of Materials Science & Engineering
National Chiao Tung University
HsinChu 300, Taiwan, ROC
Dr. L.-J. Li
Department of Physics
National Tsing Hua University
Taiwan, ROC

DOI: 10.1002/adma.201202920

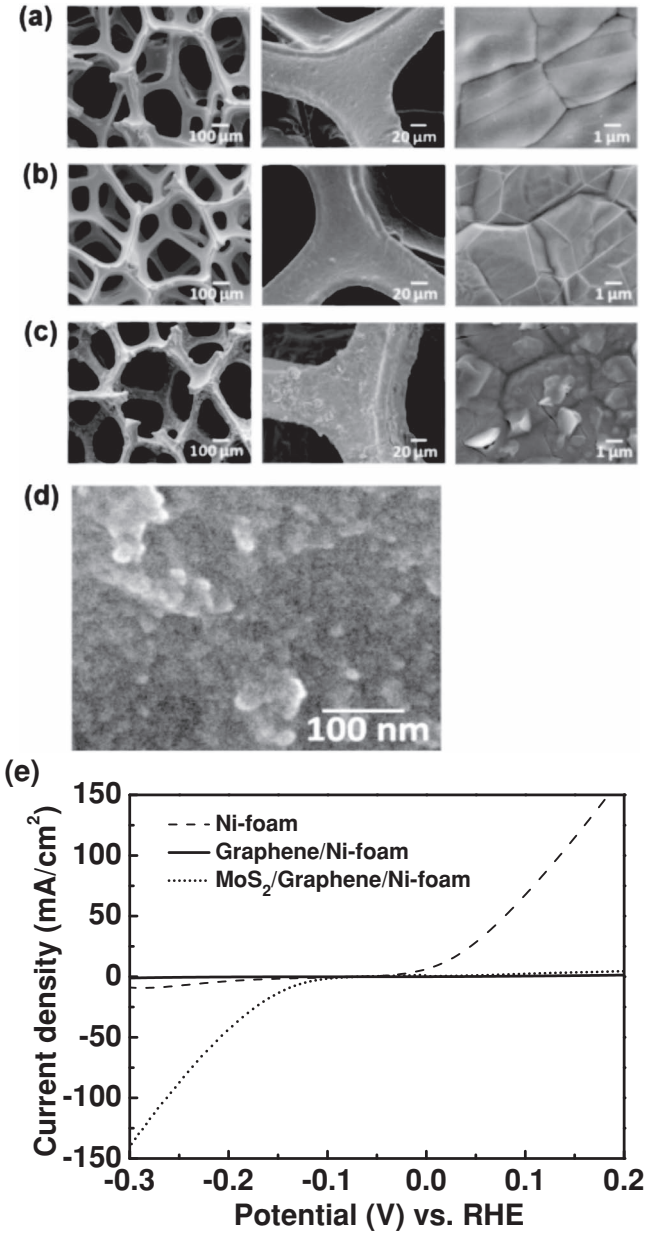

Figure 1. a) SEM images for the as-obtained Ni foam, where sub-millimeter pores can be clearly observed. b) SEM images of the Ni foam surfaces after graphene layers are grown. c) SEM images of the graphene-protected Ni foam grown with the MoS_x annealed at 120 °C. d) High resolution SEM image of the sample in shown in (c). e) The polarization curves of the as-obtained Ni foam electrode (dotted line), the graphene-protected Ni foam electrode (solid line), and the graphene-protected Ni foam electrode with MoS_x grown at 120 °C (dotted line). The measurements were performed in a 0.5 M H_2SO_4 solution. The current was normalized by the geometrical area of the Ni foam.

electrocatalytic HER is normally performed in acidic solutions, where the Ni foam is not stable in acid. The dashed line in Figure 1d displays the polarization curve of the as-obtained Ni foam electrode in a 0.5 M H_2SO_4 solution, where the oxidative potential (positive potential vs reactive hydrogen electrode, RHE) induces a high current which indicates the dissolution of Ni in acidic solutions. After CVD graphene layers are deposited on Ni foam surfaces, the oxidative current is significantly suppressed (solid line). This observation proves that the CVD graphene is able to protect the Ni foam from oxidative corrosion in acidic environments. The dotted line in Figure 1d demonstrates the polarization curve of the graphene-protected Ni foam electrode grown with MoS_x (annealed at 120 °C), where the negative current at a negative potential is the current associated with the HER. The inset is a photograph taken during the electrocatalytic hydrogen reduction (potential: –0.2 V), where the large (millimeter size) H_2 bubbles are formed due to ease of merging of the evolved tiny H_2 gas bubbles in the pores of the 3D electrodes.

Figure 2a shows the polarization curves (measured current normalized by the geometrical area of the Ni foam) for the MoS_x prepared at different annealing temperatures. It is observed that the HER efficiency exhibits a maxima at $T = 120$ °C and it decreases with the further increase in annealing temperature. The inset plots the current density at the applied potential of 0.2 V as a function of annealing temperature. It is noted that the geometrical size of the Ni foam and the loading amount of the MoS_x are similar for each annealing temperature (see Table S1, Supporting Information, for details). Figure 2b replots the polarization curves using the measured current normalized by loading weight of MoS_x and the electrochemical surface area (ESA) (see Table S1 for details). The ESA was determined by the reported method.[41,42] The HER efficiency still shows a maxima at $T = 120$ °C, consistent with Figure 2a.

A Tafel plot is normally used to evaluate the efficiency of the catalytic reaction. Table S2 and Figure S2, Supporting Information, show the HER activity of the graphene-protected Ni foam electrodes decorated with MoS_x prepared at different temperatures. These values were derived from the polarization measurements. Figure 2c shows that the Tafel slope for the electrodes decorated with the MoS_x formed at 120 °C is the smallest (≈42.8 meV dec^{-1}). The classical theory of hydrogen generation[34,43,44] suggests that a Tafel slope of ≈40 meV dec^{-1} indicates a low surface coverage of adsorbed hydrogen and the reaction is as shown in Equation (1) and (2). The MoS_x prepared at a higher annealing temperature, e.g., 300 °C, results in a lower HER efficiency and the reaction mechanism moves to a larger surface coverage and the reaction follows Equations (1) and (3).[34,35] Also, these results suggest that the different current density values actually originate from the various catalytic activities of MoS_x catalysts formed at different temperatures.

$$H_3O^+ + e^- + \text{catalyst} \longrightarrow \text{catalyst-H} + H_2O \quad (1)$$

$$H_3O^+ + e^- + \text{catalyst-H} \longrightarrow \text{catalyst} + H_2 + H_2O \quad (2)$$

$$\text{catalyst-H} + \text{catalyst-H} \longrightarrow 2\,\text{catalyst} + H_2 \quad (3)$$

To understand the differences between the MoS_x catalysts prepared at various temperatures, XPS was adopted to characterize the chemical bonding structures. **Figure 3** displays the detailed XPS scans for the Mo and S binding energies for these MoS_x catalysts. The MoS_x prepared at 300 °C exhibits two characteristic peaks at 232.1 and 228.9 eV, attributed to the

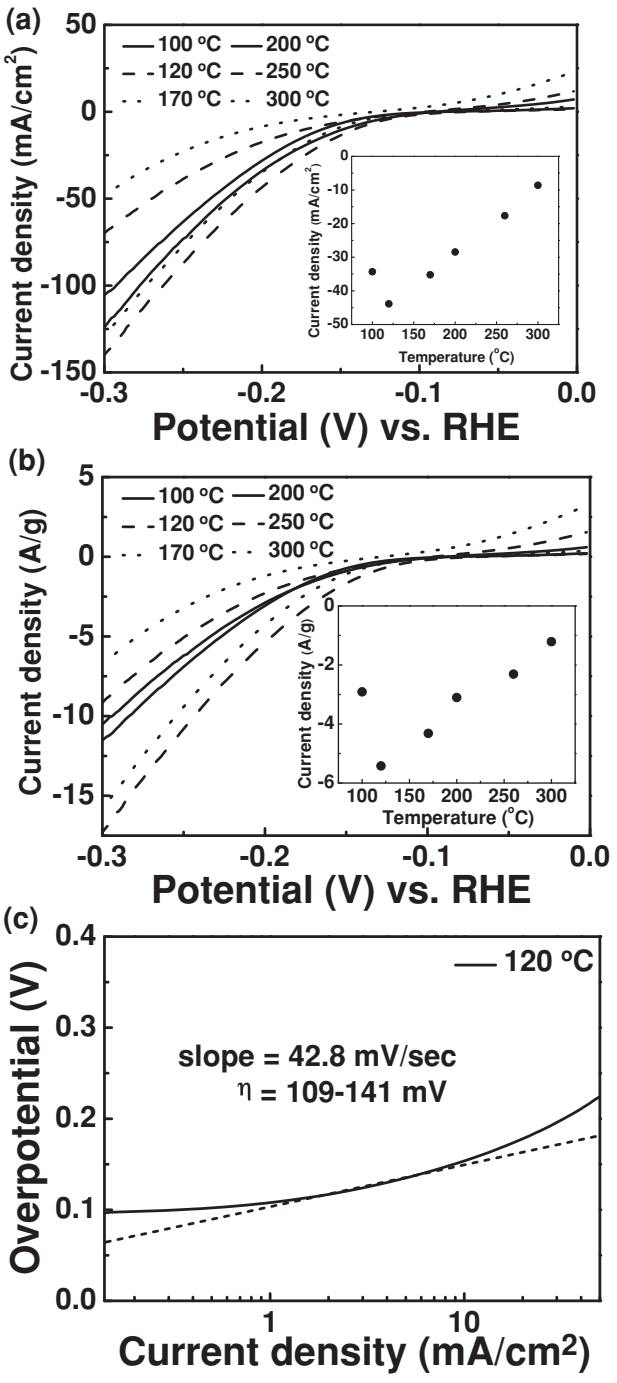

Figure 2. Polarization curves for the MoS_x prepared at different annealing temperatures, where the current density is normalized by a) geometrical area of the Ni foam, and b) both the loading weight of MoS_x and the electrochemical surface area (ESA). c) Tafel plot for the MoS_x grown (at 120 °C) on a graphene-protected Ni foam.

Mo $3d_{3/2}$ and $3d_{5/2}$ binding energies for Mo^{4+}.[45–47] The peaks, corresponding to the S $2p_{1/2}$ and $2p_{3/2}$ orbitals of divalent sulfide ions (S^{2-}) are observed at 162.9 and 161.8 eV.[45–47] The stoichiometric ratio (S:Mo) estimated from the respective integrated peak area of XPS spectra is close to ≈2.09, suggesting that the structure is close to MoS_2.[48,49] When the annealing temperature is lowered, in addition to the XPS peaks for the MoS_2 structure, other sets of peaks are also observed. The observation of Mo $3d_{3/2}$ and $3d_{5/2}$ binding energies at 233.1 and 230 eV suggests the presence of Mo^{5+} ions.[45–47] Meanwhile, the S $2p_{1/2}$ and $2p_{3/2}$ energies at 164.3 and 163.2 eV suggest the existence of bridging S_2^{2-} or apical S^{2-}.[45,46] Although it is not possible to exclusively identify the ratio between these sulfur species due to their similar binding energies, the presence of these higher energy peaks indicate that the active HER species are likely related to these species. It is noted that the HER efficiency for highly crystalline MoS_2 obtained at 1000 °C is very low (Figure S3, Supporting Information), indicating that MoS_2 is less active for electrocatalytic HER. The S:Mo atomic ratios for these samples are labeled in Figure 3, from which we conclude that the structure of the MoS_x obtained at lower temperatures such as 100, 120, and 170 °C is stoichiometrically close to Mo_2S_5. The transmission electron microscopy (TEM) and X-ray diffraction analyses reveal that all the MoS_x materials obtained in the temperature range of 100 to 300 °C are basically amorphous (data not shown). This evidence implies that the higher HER efficiency is related to the presence of bridging S_2^{2-} or apical S^{2-} in amorphous states. We have also examined the XPS spectra for the MoS_x sample prepared at 120 °C after electrocatalytic hydrogen generation reaction (Figure S4, Supporting Information). Interestingly, the the content of Mo^{6+} and Mo^{5+} in a MoS_x material is increased after electrocatalytic reaction even though the Mo^{6+} oxidation state does not exist before the electrocatalytic reaction, in good agreement with the groups of Tang[30] and Vrubel.[45] However, the binding energies of S^{2-}, located at 161.7 and 162.8 eV, and energies for bridging S_2^{2-} or apical S^{2-}, located at 163.2 and 164.3 eV, are still present after electrocatalytic reactions, not showing any apparent change in XPS peak profile.

Figure 4 shows the measured hydrogen gas evolution rate (mmol of H_2 normalized by the weight of the catalyst and the geometrical area of the graphene-protected Ni foam) for the MoS_x prepared at various temperatures. The H_2 evolution rate normalized by catalyst weight and ESA is shown in Figure S5, Supporting Information, for comparison. The highest hydrogen production rate we have achieved so far is around 13.47 mmol $g^{-1}cm^{-2}$ h^{-1} (302 mL $g^{-1}cm^{-2}$ h^{-1}) at a potential of V = 0.2 V for the MoS_x obtained by annealing at 120 °C. Note that the current density for the sample operated at 0.2 V is around 45 mA cm^{-2}. Moreover, Figure S6, Supporting Information, shows the current density as a function of hydrogen evolution time. The hydrogen production efficiency is superior to several recent HER reports based on MoS_3 particles,[45] amorphous MoS_x prepared by electro-polymerization,[50] and MoS_2/reduced graphene oxides.[34]

The advantage of using a 3D Ni foam as an electrode is that the loading weight of the MoS_x catalyst is larger than other carbon-based electrodes such as carbon paper, carbon cloth, and graphite mats as detailed in Table S3, Supporting Information. **Figure 5** compares the polarization current density (normalized by ESA) for the MoS_x grown on various carbon electrodes, where the graphene-protected 3D Ni foam exhibits the highest current density. The superior performance is attributed to the relatively high catalyst loading weight as well as the relatively

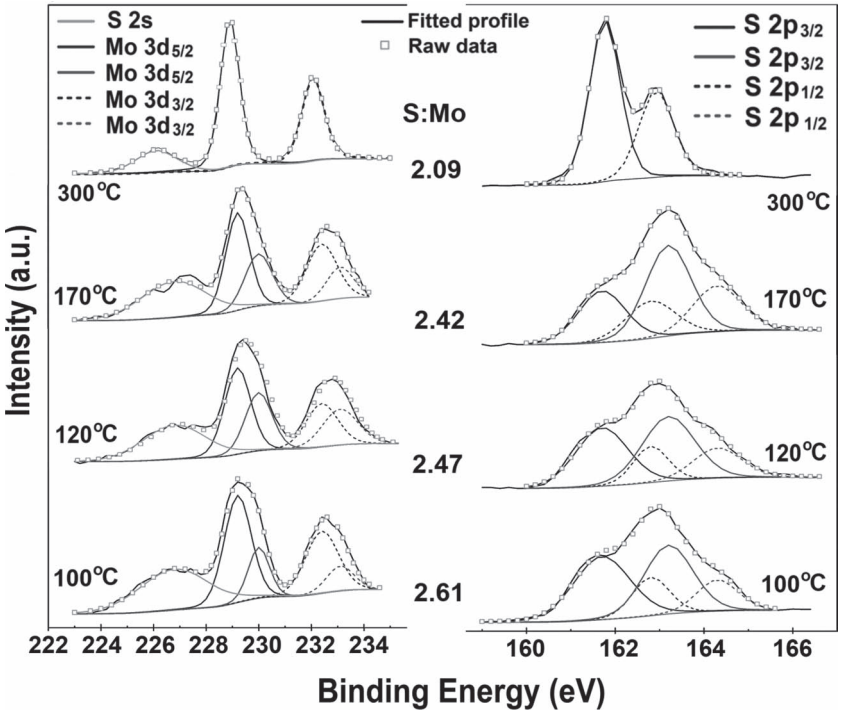

Figure 3. XPS scans for the Mo and S binding energies of various MoS_x catalysts.

lower resistance of the electrodes: the sheet resistance of these carbon electrodes is listed in Table S3.

In summary, a 3D Ni foam deposited with graphene layers on its surface was used as a conducting solid support to load MoS_x catalysts for electrocatalytic hydrogen evolution. The graphene sheets grown on Ni foams provide robust protection and efficiently increase its stability in acid. The hydrogen evolution rate reaches 302 mL g^{-1} cm^{-2} h^{-1} (13.47 mmol g^{-1} cm^{-2} h^{-1}) at an overpotential of $V = 0.2$ V and the catalytic species were likely related to the bridging S_2^{2-} or apical S^{2-}. The developments in graphene-based 3D electrodes may further advance the efficiency of various electrocatalytic reactions, which warrants more investigations.

Experimental Section

Growth of Graphene on Ni Foam: Three-dimensional Ni foam (110 ppi; thickness = 1.6 mm) was obtained from Nexcell battery Co. (Taiwan). The Ni foams were reduced with H_2 flow (100 sccm) at 1050 °C for half an hour in a CVD furnace before the CVD growth. For the growth of graphene layers, a mixture of CH_4 and H_2 gases (ratio 15:100; pressure 500 mtorr) was introduced to the furnace at 1050 °C for 1 h.

Thermolysis to Form MoS_x Catalysts: The graphene-protected Ni foam was immersed in an ammonium thiomolybdate solution (5 wt% of $(NH_4)_2MoS_4$ in DMF). The Ni foam was then backed on a hot-plate at 100 °C for 10 min. The MoS_x layer was then formed after subsequent annealing at various temperatures (100, 120, 170, 200, 250, 300 °C) in a H_2/Ar environment (500 torr; H_2:Ar = 20:80) in a CVD furnace.

Characterizations: Raman spectra were collected in a NT-MDT confocal Raman microscopic system (exciting laser wavelength 473 nm and laser spot-size is of ≈0.5 μm). The Si peak at 520 cm^{-1} was used as reference for wavenumber calibration in Raman characterization. Chemical configurations were determined by XPS (Phi V6000). XPS measurements were performed with a Mg Kα X-ray source on the samples. The energy calibrations were made against the C 1s peak to eliminate the charging of the sample during analysis. The surface morphology of the Ni foam, graphene-protected Ni foam, and 3D MoS_x/graphene/Ni foam was examined by a field-emission scanning electron microscope (JSM-6500F). Polarization curves were recorded by an AUTOLAB pontentiostat (PGSTAT 302N) with a scan rate of 5 mV s^{-1} in a 0.5 M H_2SO_4 solution. A three-electrode configuration using an Ag/AgCl (KCl saturated) electrode as the reference electrode, a graphite rod as the counter electrode, and the 3D MoS_x/graphene/Ni foam samples as the working electrode was adopted for polarization and electrolysis measurements. In 0.5 M H_2SO_4, potentials were referenced to a reversible hydrogen electrode (RHE) by adding a value of 0.21 V.

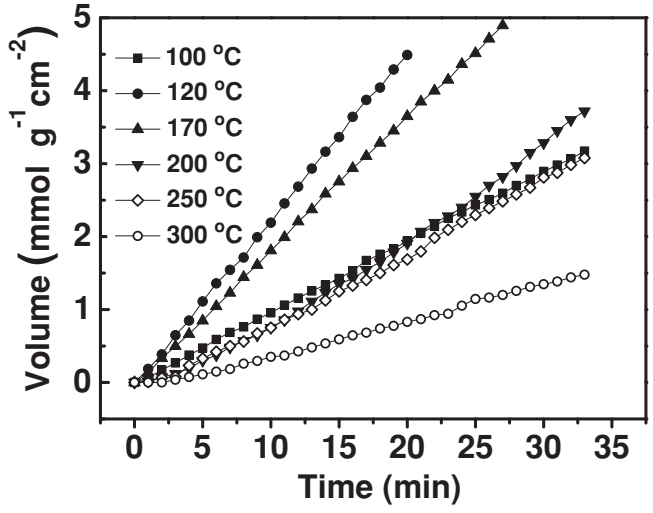

Figure 4. The measured hydrogen gas evolution rate normalized by the weight of the catalysts and the geometrical area of the graphene-protected Ni foam.

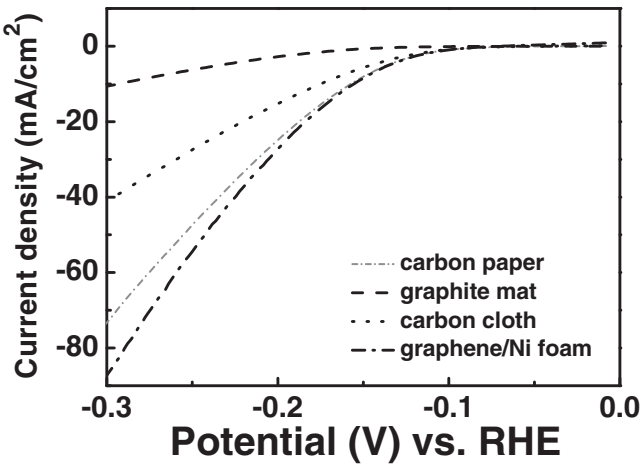

Figure 5. The polarization current density (normalized by ESA) for the MoS_x (annealed at 120 °C) grown on various carbon electrodes, where the graphene-protected 3D Ni foam exhibits the highest current density.

Supporting Information

Supporting Information is available from the Wiley Online Library or from the author.

Acknowledgements

Y. H. Chang and C. T. Lin contributed equally to this work. This research was supported by Academia Sinica (IAMS and Nano program) and the National Science Council Taiwan (NSC-99–2112-M-001–021-MY3). L.J.L. also thanks the support from NCTU, Taiwan.

Received: July 19, 2012
Revised: August 21, 2012
Published online: October 12, 2012

[1] E. Casado-Rivera, D. J. Volpe, L. Alden, C. Lind, C. Downie, T. Vázquez-Alvarez, A. C. D. Angelo, F. J. DiSalvo, H. D. Abruña, *J. Am. Chem. Soc.* **2004**, *126*, 4043.
[2] E. Navarro-Flores, Z. Chong, S. Omanovic, *J. Mol. Catal. A: Chem.* **2005**, *226*, 179.
[3] J. Greeley, T. F. Jaramillo, J. Bonde, I. Chorkendorff, J. K. Nørskov, *Nat. Mater.* **2006**, *5*, 909.
[4] M. Wu, P. K. Shen, Z. D. Wei, S. Song, M. Nie, *J. Power Sources* **2007**, *166*, 310.
[5] Y. Hara, N. Minami, H. Matsumoto, H. Itagaki, *Appl. Catal. A* **2007**, *332*, 289.
[6] Y. G. Li, P. Hasin, Y. Y. Wu, *Adv. Mater.* **2010**, *22*, 1926.
[7] K. K. Liu, W. Zhang, Y. H. Lee, Y. C. Lin, M. T. Chang, C. Y. Su, C. S. Chang, H. Li, Y. Shi, H. Zhang, C. S. Lai, L. J. Li, *Nano Lett.* **2012**, *12*, 1538.
[8] Y. H. Lee, X. Q. Zhang, W. Zhang, M. T. Chang, C. T. Lin, K. D. Chang, Y. C. Yu, J. T.-W. Wang, C. S. Chang, L. J. Li, T. W. Lin, *Adv. Mater.* **2012**, *24*, 2320.
[9] Y. Shi, W. Zhou, A. Y. Lu, W. Fang, Y. H. Lee, A. L. Hsu, S. M. Kim, K. K. Kim, H. Y. Yang, L. J. Li, J. C. Idrobo, J. Kong, *Nano Lett.* **2012**, *12*, 2784.
[10] M. G. Walter, E. L. Warren, J. R. McKone, S. W. Boettcher, Q. Mi, E. A. Santori, N. S. Lewis, *Chem. Rev.* **2010**, *110*, 6446.
[11] J. Chen, N. Kuriyama, H. T. Yuan, H. T. Takeshita, T. Sakai, *J. Am. Chem. Soc.* **2001**, *123*, 11813.
[12] B. Hinnemann, P. G. Moses, J. Bonde, K. P. Jørgensen, J. H. Nielsen, S. Horch, I. Chorkendorff, J. K. Nørskov, *J. Am. Chem. Soc.* **2005**, *127*, 5308.
[13] V. W.-h. Lau, A. F. Masters, A. M. Bond, T. Maschmeyer, *ChemCatChem* **2011**, *3*, 1739.
[14] P. Ge, M. D. Scanlon, P. Peljo, X. Bian, H. Vubrel, A. O'Neill, J. N. Coleman, M. Cantoni, X. Hu, K. Kontturi, B. H. Liu, H. H. Girault, *Chem. Commun* **2012**, *48*, 6484.
[15] A. B. Laursen, S. Kegnæs, S. Dahl, I. Chorkendorff, *Energy Environ. Sci.* **2012**, *5*, 5577.
[16] A. D. Paola, L. Palmisano, M. Derrigo, V. Augugliaro, *J. Phys. Chem. B* **1997**, *101*, 876.
[17] W. K. Ho, J. C. Yu, J. Lin, J. G Yu, P. S. Li, *Langmuir* **2004**, *20*, 5865.
[18] D. Jing, L. Guo, *Catal. Commun.* **2007**, *8*, 795.
[19] N. Ballarini, F. Cavani, L. Maselli, A. Montaletti, S. Passeri, D. Scagliarini, C. Flego, C. Perego, *J. Catal.* **2007**, *251*, 423.
[20] X. Zong, J. F. Han, G. J. Ma, H. J. Yan, G. P. Wu, C. Li, *J. Phys. Chem. C* **2011**, *115*, 12202.
[21] H. S. S. Ramakrishna Matte, A. Gomathi, A. K. Manna, D. J. Late, R. Datta, S. K. Pati, C. N. R. Rao, *Angew. Chem. Int. Ed.* **2010**, *49*, 4059.
[22] Z. Y. Zeng, Z. Y. Yin, X. Huang, H. Li, Q. Y. He, G. Lu, F. Boey, H. Zhang, *Angew. Chem. Int. Ed.* **2011**, *50*, 11093.
[23] B. Radisavljevic, A. Radenovic, J. Brivio, V. Giacometti, A. Kis, *Nat. Nanotechnol.* **2011**, *6*, 147.
[24] G. Eda, H. Yamaguchi, D. Voiry, T. Fujita, M. Chen, M. Chhowalla, *Nano Lett.* **2011**, *11*, 5111.
[25] G. M. Wang, H. Y. Wang, Y. C. Ling, Y. C. Tang, X. Y. Yang, R. C. Fitzmorris, C. C. Wang, J. Z. Zhang, Y. Li, *Nano Lett.* **2011**, *11*, 3026.
[26] X. Zong, H. J. Yan, G. P. Wu, G. J. Ma, F. Y. Wen, L. Wang, C. Li, *J. Am. Chem. Soc.* **2008**, *130*, 7176.
[27] A. Kudo, Y. Miseki, *Chem. Soc. Rev.* **2009**, *38*, 253.
[28] F. A. Frame, F. E. Osterloh, *J. Phys. Chem. C* **2010**, *114*, 10628.
[29] S. Kanda, T. Akita, M. Fujishima, H. Tada, *J. Colloid Interface Sci.* **2011**, *354*, 607.
[30] M. L. Tang, D. C. Grauer, B. Lassalle-Kaiser, V. K. Yachandra, L. Amirav, J. R. Long, J. Yano, A. P. Alivisatos, *Angew. Chem. Int. Ed.* **2011**, *123*, 10385.
[31] Q. J. Xiang, J. G. Yu, M. Jaroniec, *J. Am. Chem. Soc.* **2012**, *134*, 6575.
[32] T. F. Jaramillo, K. P. Jørgensen, J. Bonde, J. H. Nielsen, S. Horch, I. Chorkendorff, *Science* **2007**, *317*, 100.
[33] Z. Chen, D. Cummins, B. N. Reinecke, E. Clark, M. K. Sunkara, T. F. Jaramillo, *Nano Lett.* **2011**, *11*, 4168.
[34] Y. Li, H. Wang, L. Xie, Y. Liang, G. Hong, H. Dai, *J. Am. Chem. Soc.* **2011**, *133*, 7296.
[35] Z. Chen, W. Ren, L. Gao, B. Liu, S. Pei, H.-M. Cheng, *Nat. Mater.* **2011**, *10*, 424.
[36] X. H. Cao, Y. M. Shi, W. H. Shi, G. Lu, X. Huang, Q. Y. Yan, Q. C. Zhang, H. Zhang, *Small* **2011**, *7*, 3163.
[37] Y. C. Yong, X. Dong, M. B. Chan-Park, H. Song, P. Chen, *ACS Nano* **2012**, *6*, 2394.
[38] N. A. Jarrah, F. Li, J. G. van Ommen, L. Lefferts, *J. Mater. Chem.* **2005**, *15*, 1946.
[39] H. B. Dai, Y. Liang, P. Wang, X. D. Yao, T. Rufford, M. Lu, H. M. Cheng, *Int. J. Hydrogen Energy* **2008**, *33*, 4405.
[40] J. K. Chinthaginjala, L. Lefferts, *Carbon* **2009**, *47*, 3175.
[41] B. Seger, P. V. Kamat, *J. Phys. Chem. C* **2009**, *113*, 7990.
[42] W. C. Liu, H. K. Lin, Y. L. Chen, C. Y. Lee, H. T. Chiu, *ACS Nano* **2010**, *4*, 4149.
[43] J. O'M. Bockris, E. C. Potter, *J. Electrochem. Soc.* **1952**, *99*, 169.
[44] J. G. N. Thomas, *Trans. Faraday Soc.* **1961**, *57*, 1603.
[45] H. Vrubel, D. Merki, X. Hu, *Energy Environ. Sci.* **2012**, *5*, 6136.
[46] Th. Weber, J. C. Muijsers, J. H. M. C. van Wolput, C. P. J. Verhagen, J. W. Niemantsverdriet, *J. Phys. Chem.* **1996**, *100*, 14144.
[47] H. W. Wang, P. Skeldon, G. E. Thompson, *Surf. Coat. Technol.* **1997**, *91*, 200.
[48] C. N. R. Rao, A. Nag, *Eur. J. Inorg. Chem.* **2010**, *27*, 4244.
[49] C. Altavilla, M. Sarno, P. Ciambelli, *Chem. Mater.* **2011**, *23*, 3879.
[50] D. Merki, S. Fierro, H. Vrubel, X. Hu, *Chem. Sci.* **2011**, *2*, 1262.